REPORT DOCUMENTATION PAGE

AFRL-SR-AR-TR-04-

0332

1. REPORT DATE (DD-MM-YYYY)	2. REPORT TYPE	3. DATES COVERED (From-To)
11-06-2004	Final Report	09/15/2002-03/14/2004

4. TITLE AND SUBTITLE

DARPA Bio-Optic Synthetic Systems Programs: "A Novel Lens System Featuring a Highly Dynamic Focal Length."

5a. CONTRACT NUMBER

5b. GRANT NUMBER
F49620-02-1-0420

5c. PROGRAM ELEMENT NUMBER

5d. PROJECT NUMBER

5e. TASK NUMBER

5f. WORK UNIT NUMBER

6. AUTHOR(S)
Snow, Steven, A
Pernisz, Udo, C[1]
Su, Kai[1]
Grassman, Martin, P[2]
Davies, Peter, R[2]
Coles, Harry, M[3]
[1]Nishida, Fumito[1]
Lauer, Timothy, M[1]
Hannington, Jon, P[2]
Taylor, Richard, C[2]
Wilmott, Jon, P[3]

7. PERFORMING ORGANIZATION NAME(S) AND ADDRESS(ES)
(1) Dow Corning Corporation
2200 West Salzburg Road
Midland, Michigan 48686-0994
(2) Dow Corning Ltd.
Barry, Glamorgan
South Wales, U.K.
CF6 7YL
(3) Cambridge University Engineering Dept.
Cambridge University
Trumpington Street
Cambridge
CB2 1PZ
United Kingdom

8. PERFORMING ORGANIZATION REPORT NUMBER

9. SPONSORING/MONITORING AGENCY NAME(S) AND ADDRESS(ES)
Dr. Charles Lee
Air Force Office of Scientific Research
AFOSR/NL
4015 Wilson Blvd, Room 713
Arlington, VA 22203-1954

10. SPONSOR/MONITOR'S ACRONYM(S)
AFOSR

11. SPONSOR/MONITOR'S REPORT NUMBER(S)

12. DISTRIBUTION/AVAILABILITY STATEMENT
Approve for Public Release: Distribution Unlimited.

13. SUPPLEMENTARY NOTES

14. ABSTRACT
The major goal of the project was to develop an adaptive optical system featuring a radical, dynamic and reversible change in focal length using polydimethylsiloxane (silicone) science and technology. The assertion that silicone-functional mesogens (liquid crystals), where the mesogen displayed an intrinsically high birefringence, would behave similarly and yield the necessary nematic liquid crystalline mesophase in an appropriate temperature range, was demonstrated to be a robust hypothesis. The silicone portion of the materials allowed for the tailoring of both the phase behavior and miscibility to comply to the demands of the adaptive optics application. Classes of silicone mesogens, where the mesogen was either a metallomesogen or else a highly π-conjugated mesogen were successfully prepared. The metallomesogens did not display the required high birefringence ($0.2 < \Delta n < 0.5$); however, many of the conjugated mesogens did. We conclude that for the metallomesogens, the birefringence of the materials is an extremely sensitive function of the molecular structure of the material. Although many of the materials investigated demonstrated smectic phases, we were able to prepare some showing the required nematic phase. Dispersions of select mesogens in a curable silicone polymer were prepared and demonstrated an elastomeric rheology allowing for the fabrication of mechanically- and electrically-active lenses. A crude adaptive optical device was prepared using these lenses which demonstrated a dynamic, scalable and reversible focal length.

15. SUBJECT TERMS

16. SECURITY CLASSIFICATION OF: Not classified			17.LIMITATION OF ABSTRACT	18. NUMBER OF PAGES	19a. NAME OF RESPONSIBLE PERSON
a. REPORT	b. ABSTRACT	c. THIS PAGE		36	Dr. Steven A. Snow
					19b. TELEPHONE NUMBER (989) 496-6491

June 10, 2004

To:	Dr. Charles Lee	(AFOSR)
	Dr. Leonard Buckley	(DARPA)
Cc:	Dr. Fumi Nishida	(Dow Corning Corp.-Midland, MI)
	Dr. Udo Pernisz	(Dow Corning Corp.-Midland, MI)
	Mr. Tim Lauer	(Dow Corning Corp.-Midland, MI)
	Dr. Kai Su	(Dow Corning Corp.-Midland, MI)
	Mr. Jon Hannington	(Dow Corning -Barry, Wales, U.K.)
	Dr. Richard Taylor	(Dow Corning-Barry, Wales, U.K.)
	Dr. Gregg Zank	(Dow Corning Corp.-Midland, MI)
	Dr. Sian Rees	(Dow Corning-Barry, Wales, U.K.)
	Dr. Peter Lo	(Dow Corning-Midland, MI)
	Dr. Glenn Cerny	(Dow Corning-Midland, MI)
	Ms. Babette Pettersen	(Dow Corning-Seneffe, Belgium)
	Professor Harry Coles	(Cambridge University)
	Mr. Brian Russell	(Dow Corning-Midland, MI)
	Ms. Rebecca Lauer	(Dow Corning-Midland, MI)
	Mr. Doug Freitag	(Bayside Materials-Washington, DC)
Fr:	Dr. Steven Snow	(Dow Corning-Midland, MI)

Re: Final Performance Report- DARPA Bio-Optic Synthetic Systems Program: "A Novel Lens System Featuring a Highly Dynamic Focal Length". Award F49620-02-1-0420.

I. Objectives

The purpose of this AFOSR/DARPA funded research and development effort was to design and develop an adaptive optical device for military applications. The paradigm for the design effort was to use the biological eye as a model for highly dynamic optical sensing and imaging. The details of the model are reported elsewhere[1]. The team took the technical approach that radical adaptive imaging could be achieved with a device capable of simultaneous, controlled, electro-optical and mechanical-optical activity.

The general concept of the proposed lens system is shown in Figure 1 below.

---

[1] Snow, S.A.; "A Novel Lens System with Highly Dynamic and Precise Focal Length"; Dow Corning Proposal to DSO_BAA01-42. "Bio-Optic Synthetic Systems". June 10, 2002

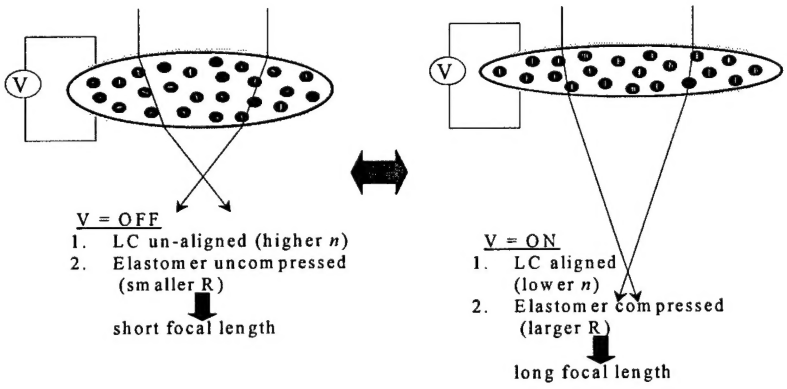

Figure 1. *The proposed dynamic focal length lens.*

The large, circular objects in Figure 1 are cross-sectional views of the proposed lens with the object on the left side representing the electrical "field off" state and the one on the right being the "field on" state. Applying the electric field to the lens compresses it, thereby changing its surface curvature. The field also aligns the liquid crystal molecules (mesogens) [in the small droplets (circles) within the lens] with the electric field. Both of these reversible effects should, presumably in an additive fashion, change the refractive power of the lens and, as a result, its field-of-view.

Specific objectives of the research and development effort included:

(1) Test the hypothesis that silicone-functional mesogens, where the mesogen is known to have a high intrinsic birefringence, would also both display a high birefringence and yield the necessary nematic liquid crystalline mesophase in an appropriate (to the application) temperature range.
(2) The silicone portion of the silicone-functional mesogen would allow for the tailoring of the phase behavior of the material.
(3) The silicone portion of the silicone-functional mesogen would allow for the tailoring of the miscibility of the mesogen in a curable silicone elastomeric matrix.
(4) Lenses would be fabricated out of elastomeric dispersions of the silicone mesogen in the curable silicone matrix.
(5) These lenses would function as dynamic focal length optical tools as prescribed by Figure 1 above.
(6) The two phenomena allowing for a change in focal length of the lens under the electric field, specifically the alignment of the mesogens and the electromechanical compression of the lens, would contribute in an additive fashion.

(7) Adaptive optical devices would be fabricated containing the lenses.

II. Status of Effort

The major goals of the original proposal were met. The assertion that silicone-functional mesogens (SFMs), where the mesogenic moiety displayed an intrinsically high birefringence, would (1) have a high birefringence, and (2) yield the necessary nematic liquid crystalline mesophase in an appropriate temperature range, was demonstrated to be a robust hypothesis. The silicone portion of the SFMs also allowed for the tailoring of the miscibility in order to comply to the demands of the adaptive optics application. Over 100 SFMs, where the mesogen portion was either a metallomesogen or else highly π-conjugated, were successfully prepared. The metallomesogens did not display the required high birefringence ($0.2 < \Delta n < 0.5$); however, many of the conjugated mesogens did. We conclude that for the metallomesogens, the birefringence of the materials was an extremely sensitive function of the molecular/electronic structure. Although many of the SFMs investigated demonstrated smectic phases, we were able to prepare four classes with the desired nematic phase. Dispersions of select SFMs in a curable silicone polymer were prepared and demonstrated an elastomeric rheology allowing for the fabrication of electromechanically-active lenses. An adaptive optical device was prepared using these lenses which demonstrated a dynamic, scalable and reversible focal length.

III. Accomplishments/New Findings

a. Mesogen Development

One method to change the refractive power of the lens is to fabricate the lens out of a material that displays a large electro-optic coefficient (dn/dE, the change of refractive index with electric field strength), which reduces to the material property of a high birefringence (Δn). The general material of choice is liquid crystals (LC, mesogens), and, due to the previous work of Wu, Bruce and others (References 2,3 and others), specifically metallomesogens or mesogens based a highly-conjugated π-electron system. One drawback of these materials is that they display the necessary nematic LC phase at temperatures too high for the planned applications. We proposed that we could lower the transition temperature by preparing polydimethylsiloxane ("siloxane" or "silicone") derivatives. We also proposed that siloxane derivatization of mesogens would make them miscible with appropriate siloxane network precursors that would enable polymer dispersed liquid crystal composites to be fabricated.

i. Silicone Functional Metallomesogens (SFM^2s)

Previous work by Bruce and co-workers[2] documented that some classes of metallomesogens demonstrated high birefringence. Based on that consideration we investigated silicone derivatives of metallomesogens (SFM[2]s), and specifically cyanobiphenyl- (CSFM) and Schiff Base (SBSFM) SFMs.

1. Cyanobiphenyl Based SFMs (CSFM[2]s)

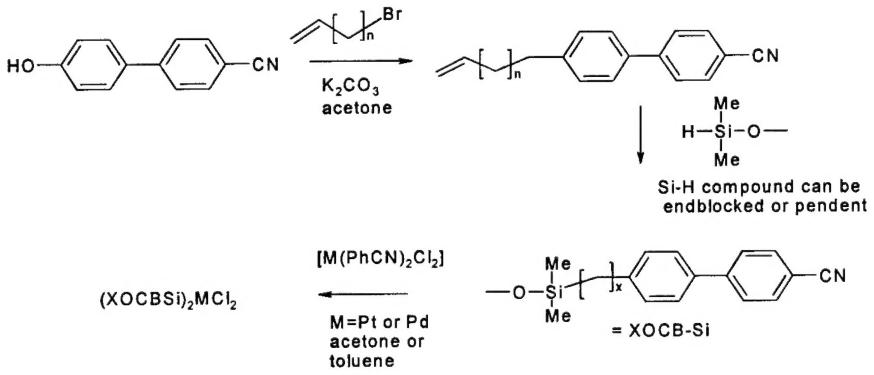

Figure 2. *Synthetic route to CSFM[2]s.*

As shown in Figure 2, CSFM[2]s were prepared using a three-step procedure. Allylation of the starting material was accomplished by the Williamson ether synthesis. This material was then siloxylated by the hydrosilylation of the allyl species by the appropriate Si-H functional siloxane. This work led to the preparation and isolation of three XOCB-Si ligands with values of $x = 4$, 8, and 11 and Si = $Me_3SiOSiMe_2$-. Reactions of these ligands with $Pd(PhCN)_2Cl_2$ yielded the CSFM[2] expected products.

LC phase characterization of these materials revealed that the CSFM[2] materials were smectic. Our lack of success in finding nematic phases within this class of mesogens, compounded by the fact that the materials synthesized often proved difficult to isolate and purify, motivated us to investigate other classes of metallomesogens. In particular, Schiff base systems were identified and investigated.

[2] (a) Bruce, D.W.; *Acc. Chem. Res.*, 2000, **33**, 831 (b) Liu, X.-H; Heinrich, B.; Manners, I.; Guillon, D.; Bruce, D.W.; *J. Mater. Chem.*, 2000, **10**, 637.

2. Schiff-Base Type SFMs (SBSFMs)

The Schiff base structure shown in Figure 3 was studied in detail; however, the resulting compounds displayed low birefringence values, in the range 0.1 to 0.2.

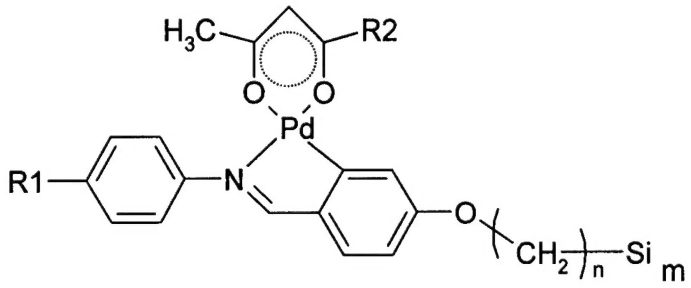

Figure 3. *The molecular structure of a Schiff-base type of silicone-metallomesogen*

We discussed this phenomenon of low birefringence with Professor D.W. Bruce at Exeter University, the pioneer in the study of metallomesogens. We concluded that subtle factors, both structural and electronic, yielded high birefringence to certain metallomesogens. Specifically, the favoured molecular electronic state is one where a high degree of electron conjugation/delocalization is present throughout the molecule. Furthermore, the d-orbitals on the metal play an important role in the maintenance of electron delocalisation. Therefore, the geometry of bonding and d-orbitals around the metal center must be in a critical alignment to allow for this delocalisation.

In an ubiquitous fashion, these systems exhibited smectic phases. Our conclusion was that the silicone moiety was "organophobic" to the extent that micro- or nanoscale phase separation of the silicone and organometallic moieties of these compounds occured within the LC phases. This phenomenon had been observed previously at Dow Corning in many mesogens containing a "simple" organic group (say cyanobiphenyl) linked to silicone.

ii. Highly Conjugated π-System Silicone Functional Mesogens (HCSFMs)

Previously, the sought-after characteristics of nematic LC phase formation and high birefringence had been extensively discussed by a number of workers in this area, in particular, Wu and coworkers[3]. In summary, the mesogen would require a highly-conjugated/delocalized π-bonded electronic structure. However, the phase transition temperatures of these materials were typically too high order to be useful in many applications. We attempted to reduce phase transition temperatures by functionalizing the mesogen with a silicone moiety.

---

[3] Wu, S.; et al.; *Appl. Phys. Lett.*, 2000, 77(7), 957-959

The first aspect of our work plan was to identify high birefringence liquid crystals based upon the following criteria:

- Highly conjugated organic mesogens, such as those reported by S.T. Wu (University of Central Florida), C. Sekine (Sumitomo Chemical Co.), and M. Hird (University of Hull). The high degree of conjugation within this organic moiety would impart significant birefringence to the hybrid mesogen.
- An oligosiloxane moiety, such as those successfully utilized by Dow Corning to tailor the properties of mesogens for smectic A scattering, electroclinic and ferroelectric liquid crystal device applications. The oligosiloxane would be used to lower the melting points and LC phase ranges of the highly conjugated organics. The high aspect ratios of the organic moieties would be expected to favour nematic phases; however, the geometry of the oligosiloxane linking unit could also be used to hinder the formation of lamellar, smectic phases. For example, by using the siloxane to couple two different organic moieties together and thus inducing a degree of asymmetry, the formation of the lower order nematic phase would be favored relative to the smectic phase. The linked siloxane would also be available to compatibilize the organic moiety with the siloxane network precursors, thus enabling the formation of siloxane-liquid crystal composite lenses.

A significant amount of work went into the preparation, isolation, purification and characterization of the HCSFMs including alkyl-functional Napthylene Cyanotolanes, alkenyloxy-functional Napthylene Cyanotolanes, **(A-Si)** siloxane-functional Napthylene Cyanotolanes, **ASiA** and **ASiB** bi-mesogens, cyclosiloxane Napthylene Cyanotolanes and silyl Napthylene Cyanotolanes. The specific reaction schemes used to synthesize these compounds are outlined in Appendix 1.

A systematic study of the liquid crystalline properties using Differential Scanning Calorimetry (DSC) and polarized light Thermo-Optic Analysis (TOA) enabled structure-property relationships to be established for the naphthylene cyanotolanes. In addition, a number of polytolanes were also prepared to enable the investigation of asymmetric systems. The phase behaviour of the HCSFM-polytolanes exhibiting liquid crystalline phase behaviour is summarised in Appendix 1, Tables 1 and 2. This extensive synthetic and characterisation study led to the elucidation of **three classes of HCSFMs which exhibited nematic phases**:

- Cyclosiloxane systems with either butyl or propyl chains linking the aromatic core to the siloxane (MG 98ER and MG103 respectively). MG103 exhibited a 20C wide nematic phase, with an underlying glass phase, illustrating the use of siloxane to hinder crystallization. No smectic phases were observed for MG103.
- Silyl systems (MG104 and 105) exhibited monotropic nematic phases (i.e. the nematic phases were only observed on cooling from the melt). No smectic phases were observed for these materials.
- The ASiA system MG110 (a polytolane) exhibited a very broad nematic phase over a 134C temperature range. The melting point of this adduct (70C) was low considering its dimeric nature. No smectic phases were observed for this material.

- The ASiB system 03RGT96 exhibited a nematic phase over a 9C temperature range. This sample had an underlying smectic phase, and formed a glass on further cooling.

The phase behaviour of these materials confirms the validity of the original hypothesis, that Si-modification can be used to reduce the melting points of highly conjugated systems and that nematic phases can be achieved by careful control of the molecular structure of the silicone and organic moieties.

A key goal of the synthetic project was to prepare an asymmetric dimer comprising a naphthylene cyanotolane coupled to a polytolane via a short siloxane spacer. Several attempts were made to prepare such an ASiB system, but this was not achieved before the closure of the project. Promising results from naphthylene/cyanotolane dimers with differing alkyl chain spacer lengths (MG95, which has a low melting point of 56C) and the presence of a nematic phase for 03RGT96, indicated that the asymmetric approach has merit; however, further work is required to optimize the phase type, temperature range and birefringence.

A large number of mesogenic materials were prepared during this project, and, based on the attaining the project goal of yielding near-room temperature nematic phases, there was motivation to prepare eutectic mixtures via formulation with organic, or siloxane-organic mesogens. As an example, the phase modification of MG110 using a conventional organic liquid crystal formulation (Merck E7) is illustrated in Table 1. This data confirms that the polytolane-siloxane adducts are miscible with a cyanobiphenyl-based organic nematic formulation, resulting in the melting point of the MG110 being reduced from 70C to below 0C. Eutectic mixtures comprising both organic and siloxane modified highly conjugated organic systems should be further studied in the future.

Note that enthalpies are given in J/g)

Sample	Si Moiety	Cycle	Phase Behaviour
MG110 FW = 908	TMDS	Heat Cool	Cr → 64C (15.0) and 70C (12.4) → N →204C (2.4) → I I → 197C (1.01 → N → 28.1C (12.9) and 23C (3.3) → Cr
MG110/E7	NA	Heat Cool	Cr → -4.7C (9.3) → N → 118.4C (3.7) → I I → 118.2C (2.8) → N → -10C (0.5) Sa →.-12.9C (5.8) → Cr
E7	NA	-	S → <-20C → N → 61C → I Source: Merck Data Sheet

Table 1. *Liquid Crystal phase behaviour of a 50:50 (w/w) blend of MG110 and the nematic formulation E7.*

Miscibility studies using a batch of butyloxy naphthylene cyanobiphenyl (MG97A) and the key component of a UV-curable siloxane formulation (ultimately used to form an elastomeric lens) **highlighted the significant enhancement in miscibility following oligosiloxane modification of the mesogen.** The "purely organic" MG97A phase separated (Temperature Induced Phase Separation) at 72.5C, at only 2% loading (w/w) of the UV-curable siloxane. However, phase separation was not observed until 30C in a mixture containing 30% (w/w) of the heptamethyltrisiloxane adduct MG88F2 with the UV-curable siloxane. Thus, oligosiloxane modification of organic mesogens could be used to enable UV-curable siloxane mixtures with high mesogen loadings to be prepared prior to phase separation upon polymerisation (Polymerisation Induced Phase Separation). This phase separation process was necessary in order to form the elastomeric, polymer dispersed liquid crystal matrix required for the lens.

b. Mesogen Characterization

The birefringence of the SFMs exhibiting liquid crystal phases was investigated by our collaborative partners, Prof H.J. Coles and Dr J. Willmott, at Cambridge University. A number of techniques were developed for the determination of birefringence as both a function of temperature and of wavelength. The techniques used included i) an Abbe refractometer, ii) the hollow prism method, iii) the interference method, and iv) the rotating analyzer method. Experimental details of these techniques are given in Appendix 3.

The organic precursor molecule MG92, which had a nematic phase, was used to illustrate the protocol for the determination of birefringence. The structure of MG92 is shown below.

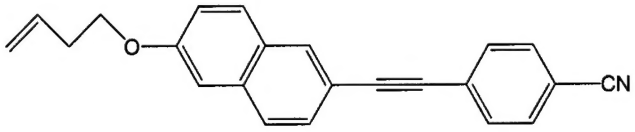

Figure 4. *The molecular structure of the mesogen MG92 (Dow Corning internal nomenclature)*

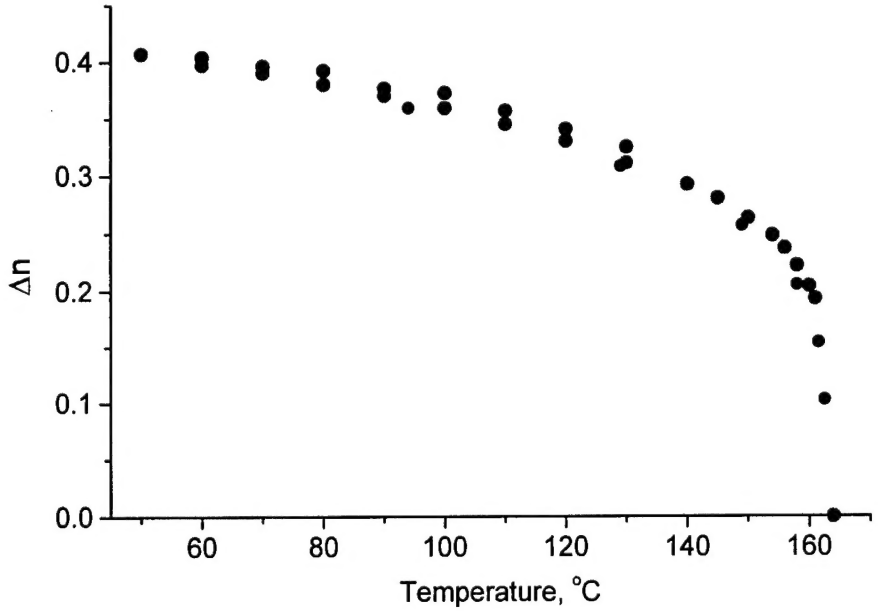

Figure 5. *MG 92-temperature dependence of the birefringence for 632 nm. measured with different methods: Rotating Analyser Method (black), Interference Method for Plane-parallel Nematic Cell (red), Hollow Prism Method (blue).*

The birefringence data for MG92, obtained using a range of techniques, is in good agreement (comparing the different techniques). The interference and rotating analyzer techniques (supported by the hollow prism technique) were used to characterize the bulk of the samples. Benchmarking studies were also undertaken using commercial liquid crystal mixtures and single component cyanobiphenyl liquid crystals.

Data for the extraordinary and ordinary refractive indices and the birefringence are given in Figures 6 and 7.

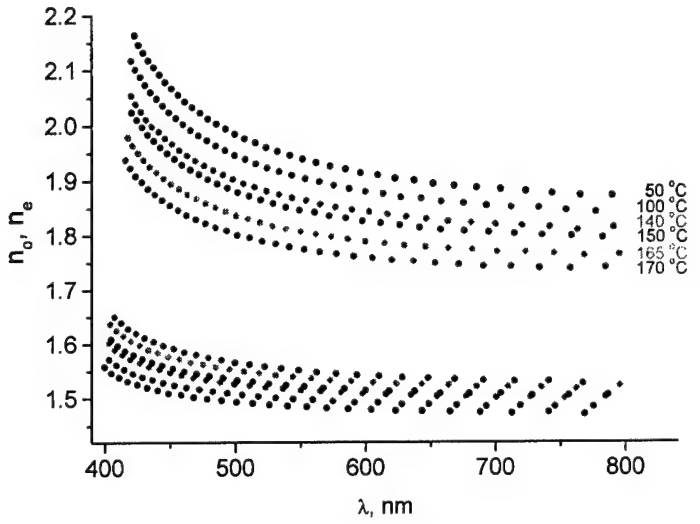

Figure 6. *Wavelength dependence (dispersion) of the extraordinary and ordinary refractive indices for different temperatures of MG 92.*

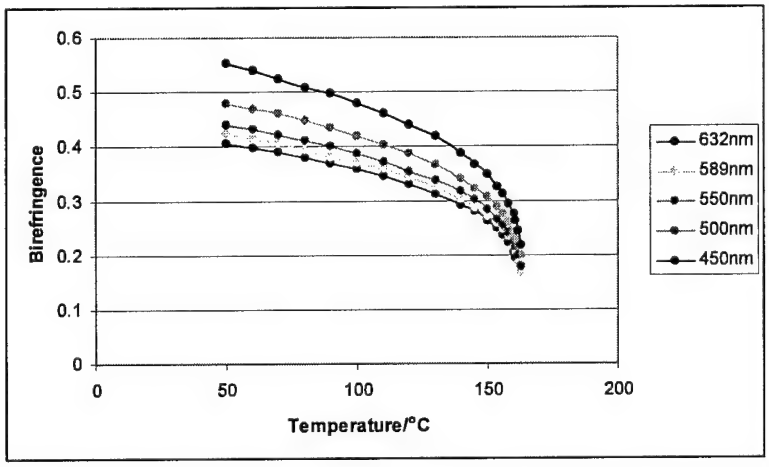

Figure 7. *Birefringence of MG92 as a function of temperature, shown at different wavelengths of light.*

This organic precursor and its butyl analogue MG97C exhibited high birefringence values when supercooled in the nematic phase. It was noted that all of the naphthylene cyanobiphenyls (organic and siloxane modified) were light sensitive and underwent slow degradation upon extended exposure to illumination from a microscope bulb, as illustrated below.

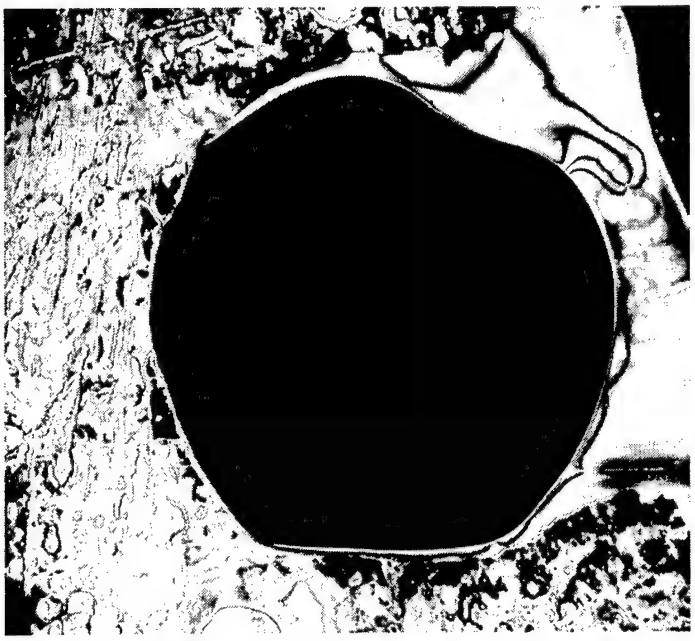

Figure 8. *MG92. After 20 minutes of illumination with a microscope bulb the clearing temperature decreased by 3 ℃. The illuminated part of the sample in the isotropic phase while the rest of the sample is in the nematic phase, the sample is at a temperature of 169.4 ℃. After two days of microscope examination of the sample the clearing temperature decreased by a total of 7 ℃.*

Data for selected Si-modified naphthylene cyanobiphenyls are presented in Tables 2 and 3.

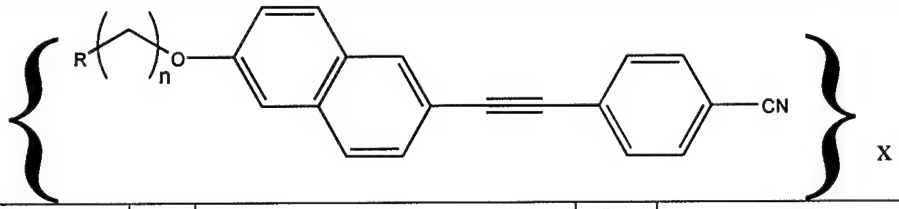

DC code	n	R	X	Birefingence, Δn
MG87-F3	4	pentamethyldisiloxane	1	0.230
MG88-F2	4	heptamethyltrisiloxane	1	0.189
MG89-F3	4	$(Me_3SiO)_2MeSi$	1	0.189
MG90-F2	10	heptamethyltrisiloxane	1	0.155
MG91-F2	10	pentamethyldisiloxane	1	0.201
MG92	2	Vinyl	1	0.335
MG93	8	Vinyl	1	0.297
MG97C	4	None	1	0.341
MG98	4	tetramethyltetracyclosiloxane	4	0.292
MG98-ER	4	tetramethyltetracyclosiloxane	4	0.271
MG104	3	trimethylsilyl	1	0.312(T_s=-15°C)
MG105	4	trimethylsilyl	1	0.365(T_s=-15°C)

Table 2. *Structure of the Naphthalene momomer (AB) and cyclosiloxane liquid crystals. The shifted temperatures are at -30°C unless otherwise state. Birefringence data was taken at 543nm.*

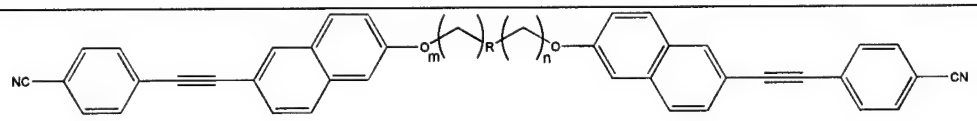

DC code	**n**	**m**	**R**	**Birefringence, Δn**
MG94	4	4	tetramethyldisiloxane	0.272
MG95	10	4	tetramethyldisiloxane	0.282

Table 3. *Structure of the bimesogenic (ABA and ABC) siloxane containing liquid crystals. Birefringence data taken at 543nm.*

Selected data is presented graphically in Figure 9.

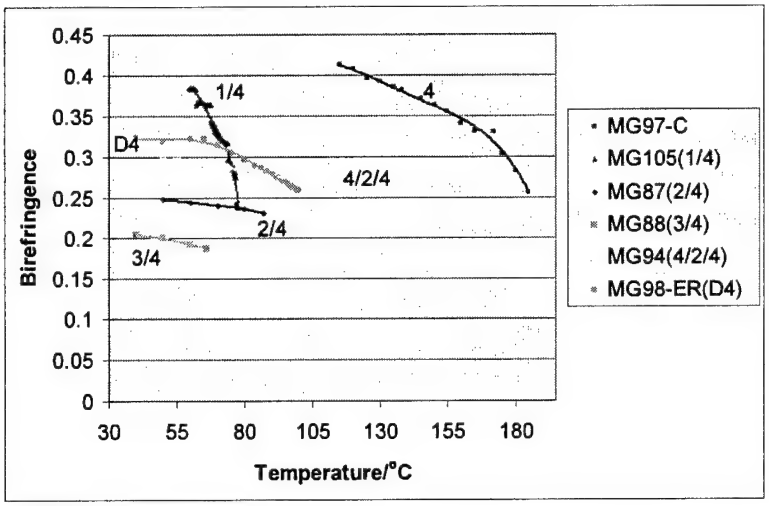

Figure 9. *Birefringence data (543nm) as a function of temperature for naphthylene based liquid crystals, generally with 4 carbon atoms in the alkoxy spacer chain.*

The data in Figure 9 highlights the influence of the siloxane structure and the ratio of the number of Si atoms to mesogen units. In general, the birefringence of the organic (MG97C, reference) falls when Si species are attached. This is somewhat surprising as one does not expect the siloxane to alter the electron delocalization, and hence the birefringence, of the organic mesogenic moiety. However, the siloxane portion tends to convert the nematic phase of the organic into a lamellar smectic phase. The reduction of birefringence suggests that the order parameter of the smectic phases are quite low. One possible explanation for the lowered order of the smectic phase is that the organic moiety may tilt in order to accommodate the increased cross-sectional area of the siloxane head group.

The silyl adduct (MG105) has a steep temperature dependence of the birefringence, as does the "purely" organic mesogen (MG97C). The temperature dependence of the birefringence is marginally reduced for the sterically constrained cyclosiloxane adduct; however, the temperature dependence is significantly reduced for the adducts which contain a free Si-O-Si linkage, whether in ASi or ASiA format. The birefringence of the 1:1 adducts (MG105, MG98ER and MG94) varies considerably depending on the type of Si species present, illustrating the ability of Si-modification to tune the properties of a given organic moiety.

c. Silicone Elastomer and Dispersion Development

The elastomeric silicone selected for lens fabrication was an olefin-functional, methylphenyl-dimethylsiloxane copolymer, which was cured in the presence of Si-H-containing cross-linking agents and platinum catalysts. Mesogen dispersions of this

material, which were optically clear and displayed a significant EO coefficient [Δn = 1.04×10^{-6} V^{-1} cm^{-1} for a 30% dispersion of K15 (commercial mesogen)-in-silicone] were prepared and used for the lens fabrication development studies.

d. Optical Device Development

i. Overview

Taking advantage of the poor adhesion of silicone to glass, a lens fabrication method was developed using a commercial concave glass lens as a mold. This allowed for the use of a high precision mold at low cost . Commercial optical lens have superb surface quality, proper surface curvature, and, most importantly, a wide range of sizes and focal lengths are available.

The lenses used for molding were purchased from the Rolyn Optics Company. The most commonly used mold lens was a bi-concave lens with a 50 mm diameter and a focal length of 53 mm; however, other lenses were also used to obtain different values for the focal length of the as-cast silicone lens. The cast silicone lens was plano-convex (i.e., flat on one side and convex on the other). Typical size of the fabricated lens was 20 mm in diameter with a center thickness of about 1.5 mm.

A key step in fabricating the electric field-actuated lens was establishing a method to coat a thin metal layer onto elastomeric silicone polymer-dispersed liquid crytals (SiPDLC). The metallic coating on silicone served as both an electric contact and optical reflector. Although metallization on silicone is commonly carried out in microelectronic processing, coating a large area (greater than 1 cm^2) of flawless metal layer on a high thermal expansion material (i.e., a silicone) was found to be a challenging and difficult task.

ii. Metal Lens Coating Development

Metal cracking can be an issue in metal-on-elastomer coatings. Due to its high ductility, direct coating of gold onto a silicone elastomer appeared to circumvent the cracking issue. However, the resulting metal coating lacked sufficient adhesion to cured SiPDLC- the gold was easily removed upon gently touching the metal. Fortunately, aluminum (as thick as 100 nm) was found to adhere well to the cured silicone with sufficient ductility to yield a crack resistant metal coating and sufficient reflectivity to function as an optical mirror. Further refinement of the deposition process was realized when a very thin layer of gold was coated on the outer surface of the aluminum for passivation and pinhole mitigation.

Despite identification of a good priming metal (Aluminum), conventional vacuum evaporation of most metals onto the SiPDLC still presented a number of difficulties including (1) Gross mismatch of the coefficients of thermal expansion of the SiPDLC and the metal, and (2) Migration of the liquid crystals to the surface of the elastomer under the high vacuum conditions necessary for metal deposition. To circumvent these problems, a UV curable

SiPDLC formulation was implemented utilizing a photo-generated, radical-catalyzed reaction between $CH{=}CH_2$ and SH as described in a U.S. provisional patent application[4]

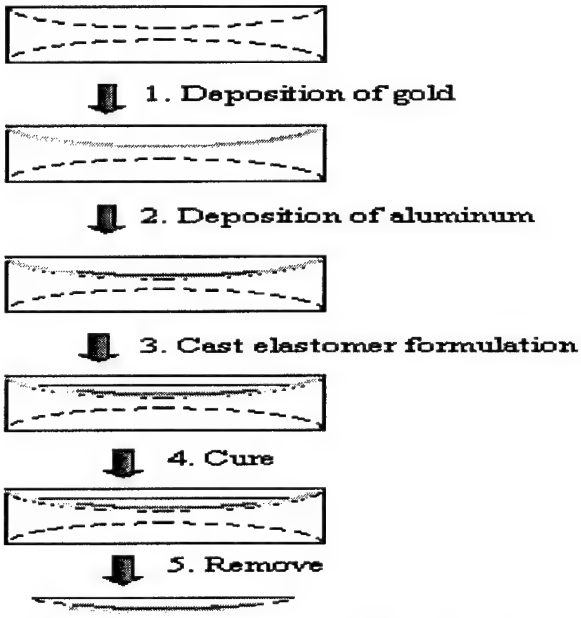

Figure 10. *Steps for coating metal onto a temperature and vacuum sensitive silicone elastomer via "Metal Transfer Coating".*

The general scheme developed for coating metal onto silicone PDLC is depicted in Figure 10. The metal coating is deposited onto the SiPDLC by first coating the mold with the metal and then casting a curable polymeric precursor on top of it. This laminate is then demolded. This process takes advantage of the poor adhesion of the gold to glass thereby using gold as a "release" layer.

The key feature of this approach is the use of radiation cure at a controlled temperature in order to compensate for any dimensional change associated with cure chemistry. The cure temperature is deliberately sub-ambient. Post-curing, the sample as allowed to reach room temperature and thermal expansion counteracts cure-induced shrinkage resulting in minimal dimensional change at its surfaces and hence a smooth metal coating. For the present UV-curable PDLC formulation, radiation cure was carried out at 4 °C using an O_2–poor atmosphere to avoid vinyl–SH reaction inhibition.

[4] Su, K.; et al.; "Silicone Composition and Polymer Dispersed Liquid Crystals"; U.S. Provisional Patent Application DC 5176

iii. Lens Performance Demonstration

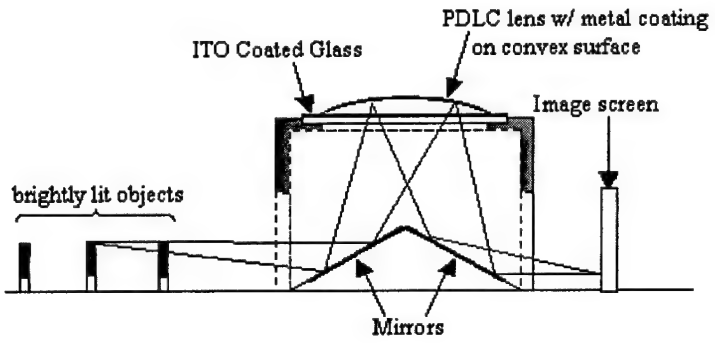

Figure 11. *Conceptual design of the unit to demonstrate the electric field actuated silicone PDLC lens. Figure shows lens*

Figure 11 illustrates the design of the demonstration unit utilizing the imaging lens in a reflective mode. An electric potential difference is applied between the metal electrode (top, curved portion of the lens) and the ITO counter-electrode (bottom, flat portion of the lens). The light entering from the left hand port reflects on a mirror mounted in the box, enters the silicone lens and reflects off the metal layer coated on its convex surface, and exits at the other port.

The actual unit was built at our Dow Corning internal machine shop (Figure 12). The only difference was in the object to be imaged – instead of different colored objects, a laser pointer casting the image of an arrow was used. The constructed device was secured on a breadboard along with fixture for top electrode contact and posts for supporting the laser pointer. A separate power supply (Phenix Technologies Model PAD10-25) was used for applying electrical bias.

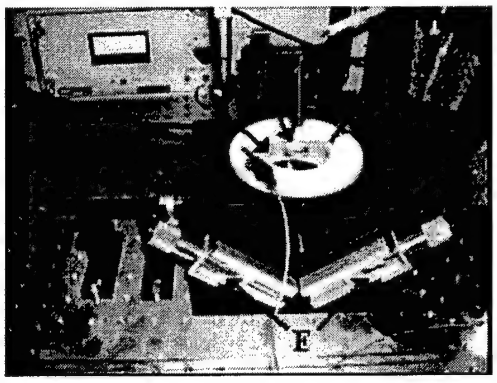

Figure 12. *Photograph of demonstration unit used at the review meeting. A: arrowed laser pointer; B: PDLC lens; C: ITO coated glass; D top electrode support; E: mirror angle adjustment knob (mirrors in the black box); F: image exit port*

A internally-developed SiPDLC material was used for demonstration. The SiPDLC was cast into a lens 25 mm diameter with a center thickness of about 1.5 mm. An excellent image of the laser pointer arrow could be seen reflected off the mirrored lens (i.e., metal coated lens) as seen in the far left photograph in Figure 13. This image was distorted upon application of the

electric potential and the level of distortion scaled with the electic field up to (at least) 3500 V (Figure 13). The phenomenon of distortion of the arrow was reversible and one could cycle a number of times through distortion and reconstitution of the image. Since the lens thickness is approximately 1.5 mm, this corresponds to electrical field of only 2.3 V/μm which is comparable to typical bias value applied across a common liquid crystal cell.

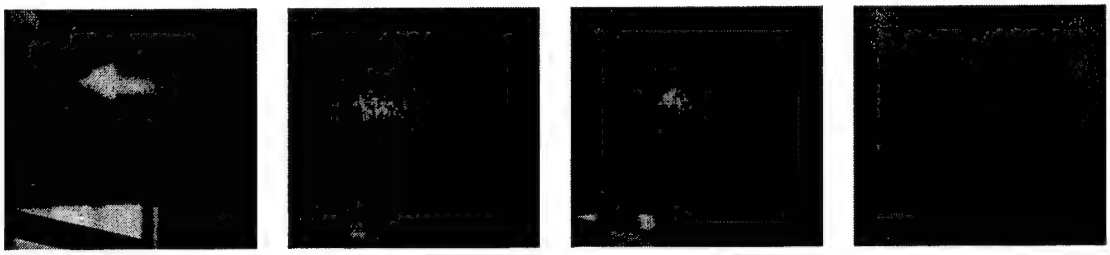

2000 V 2500 V 3000 V 3500 V

Figure 13. *Image distortion observed through PDLC lens as function of externally applied electric tension. Dim arrow seen above the reflected image is the front face reflection off of the glass substrate (not going through PDLC). The distortion is reversible with voltage change*

We demonstrated that the change of focal length of the lens in the range of 0-3500 V was 0.7 mm, a 4% change. Most of this change came from the electro-mechanical distortion of the lens. Further analysis of the electro-optic effect can be found in Appendix 4.

e. Summary-Key Points

i. Over 100 mesogens, the great majority containing silicone, were synthesized, isolated, purified and characterized.
ii. A very striking tendency on the part of SFMs to form smectic LC phases. This appears to be due to the "organophobic" nature of the silicone moiety, allowing for micro-phase separation within the LC mesostructure.
iii. However, tenacious efforts led to the synthesis of four classes of nematic SFMs.
iv. HCSFMs were synthesized that displayed moderately high birefringence, $0.2 < \Delta n < 0.4$ near ambient temperature.
v. As hypothesized, the silicone portion of the silicone mesogens reduced the liquid crystal phase transition temperatures and allowed for tailoring of the miscibility in silicone media.
vi. Silicone-polymer dispersed LCs were cured and shaped into functioning lenses.
vii. A crude, although successful, demonstrator adaptive optical device was designed and developed.
viii. Reversible ("adaptive") refraction and imaging was realized with the device. As hoped-for, the optical phenomena were a function of electric field strength.

IV. **Personnel Supported**

The following personnel at Dow Corning Corporation and Cambridge University were supported by the funds from this research and development grant.

a. **Cambridge University**
   i. Dr. John Willmott
   ii. Professor Harry J. Coles

b. **Dow Corning Corporation**
   i. Dr. Fumito Nishida
   ii. Dr. Udo Pernisz
   iii. Mr. Tim Lauer
   iv. Dr. Kai Su
   v. Mr. Jon Hannington
   vi. Dr. Richard Taylor
   vii. Dr. Martin Grassman
   viii. Mr. Peter Davies
   ix. Dr. Steven Snow

V. **Publications**
None to date

VI. **Meetings and Conferences**
None attended to date

VII. **Consultations**

a. Professor S.T. Wu, University of Central Florida
b. Professor D.W. Bruce, Exeter University

VIII. **Technology Transfer**

Nematic silicone-containing liquid crystal materials have been transferred to Professor Harry Cole's research group at Cambridge University. Professor Cole's group is currently involved with the construction of a wide array of electro-optic devices, not necessarily adaptive lenses, based on this technology.

IX. New Discoveries, Inventions or Patent Disclosures

a. "Pentamethyldisiloxane Liquid Crystals and Associated Materials" Invention Disclosure in progress
b. F. Nishida, T.M. Lauer, U.C. Pernisz, US provisional patent application "Use of Aluminum as Primer for Metallization on Cured Polysiloxanes" (Serial Number 60/520,598), filed 17 Nov. 2003.
c. F. Nishida, T.M. Lauer, U.C. Pernisz, US provisional patent application "Method of Forming Metal Coatings on Cured Polysiloxanes" (Serial Number 60/520,600), filed 17 Nov. 2003.

X. Appendices

Appendix 1 – Reaction Schemes for Highly Conjugated Silicone Functional Mesogens (HCSFMs)

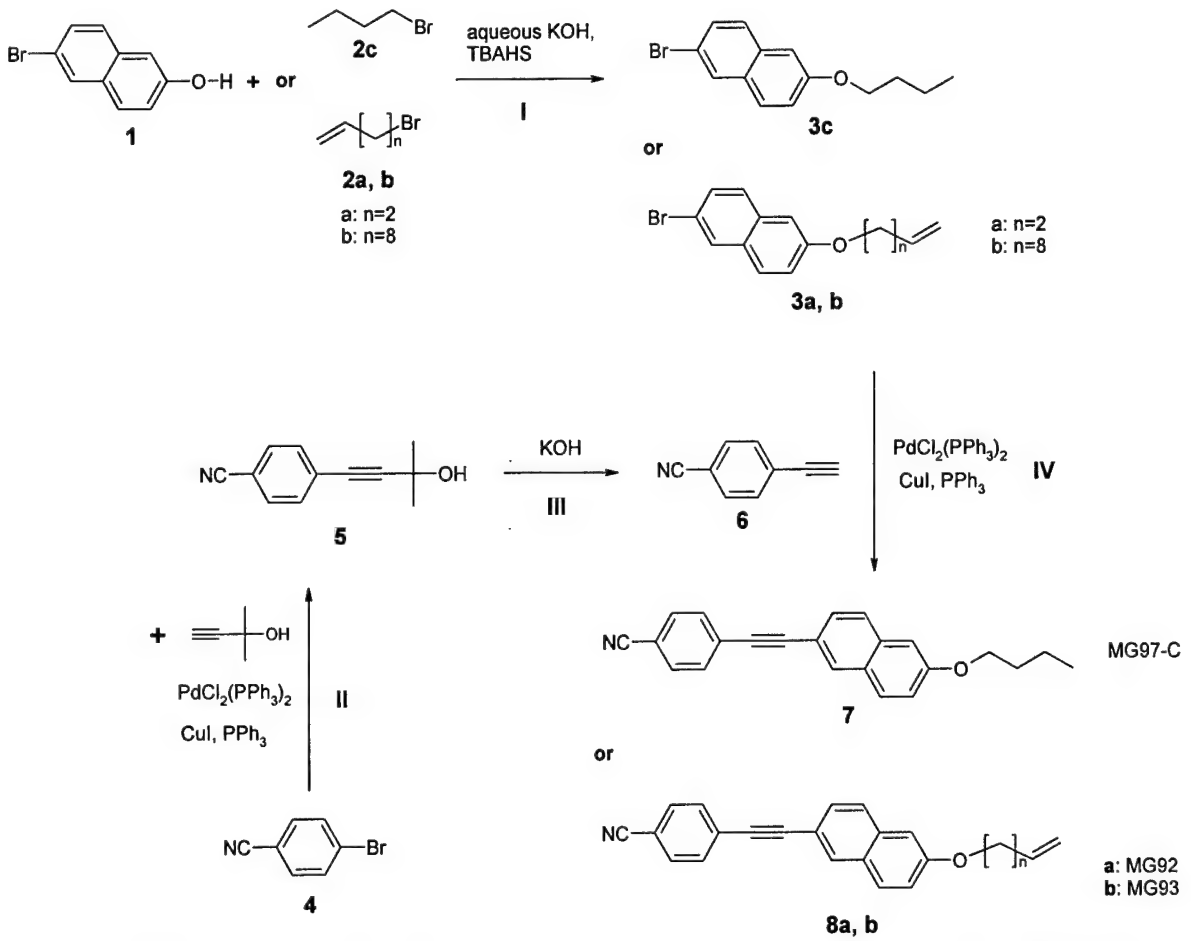

Scheme A1-1. *Synthetic pathway to alkyl-functional and allyloxy-functional napthylene cyanotolanes 7 and 8a,b.*

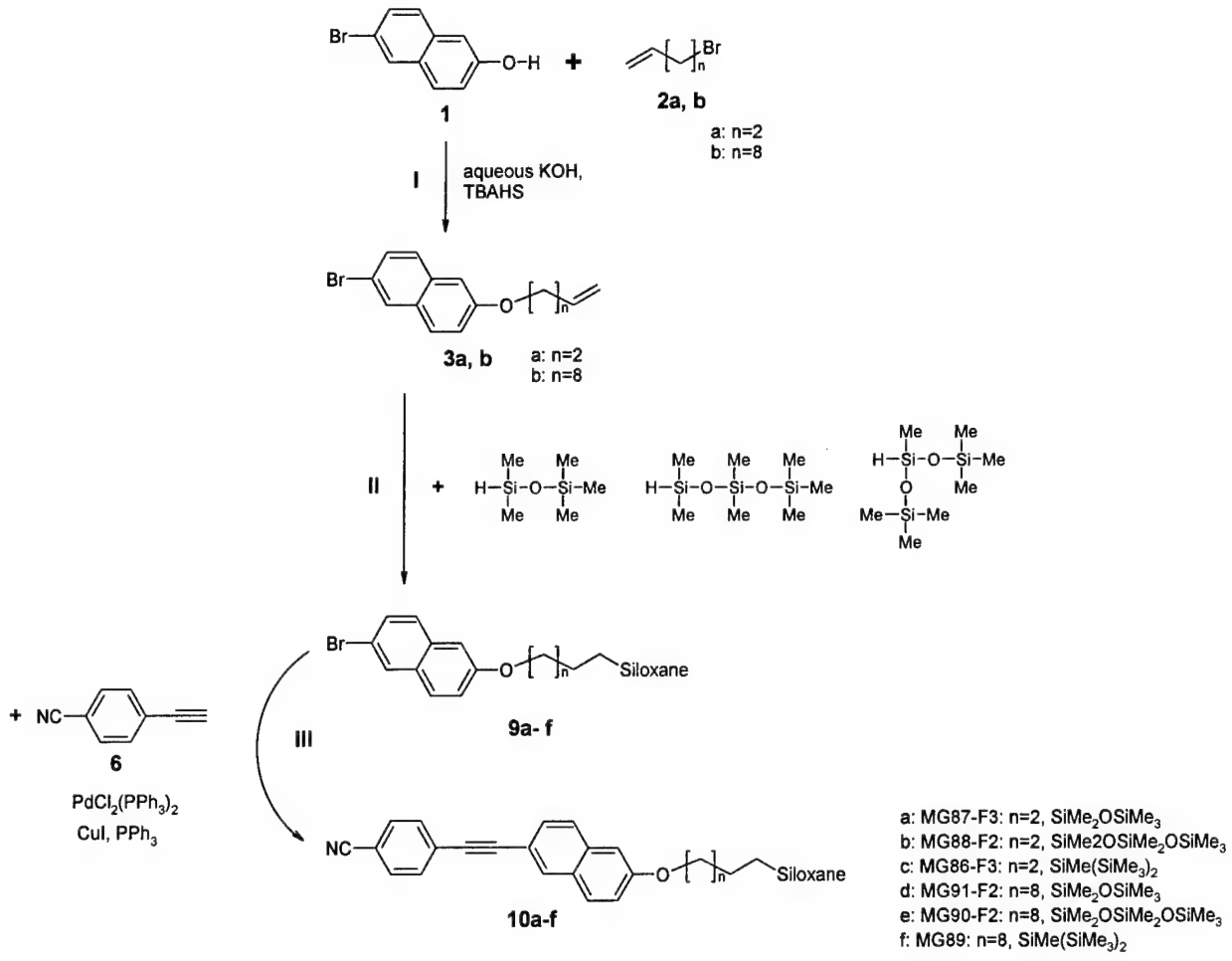

Scheme A1-2. *Synthetic pathway to siloxane-functional napthylene cyanotolanes 10a-f*

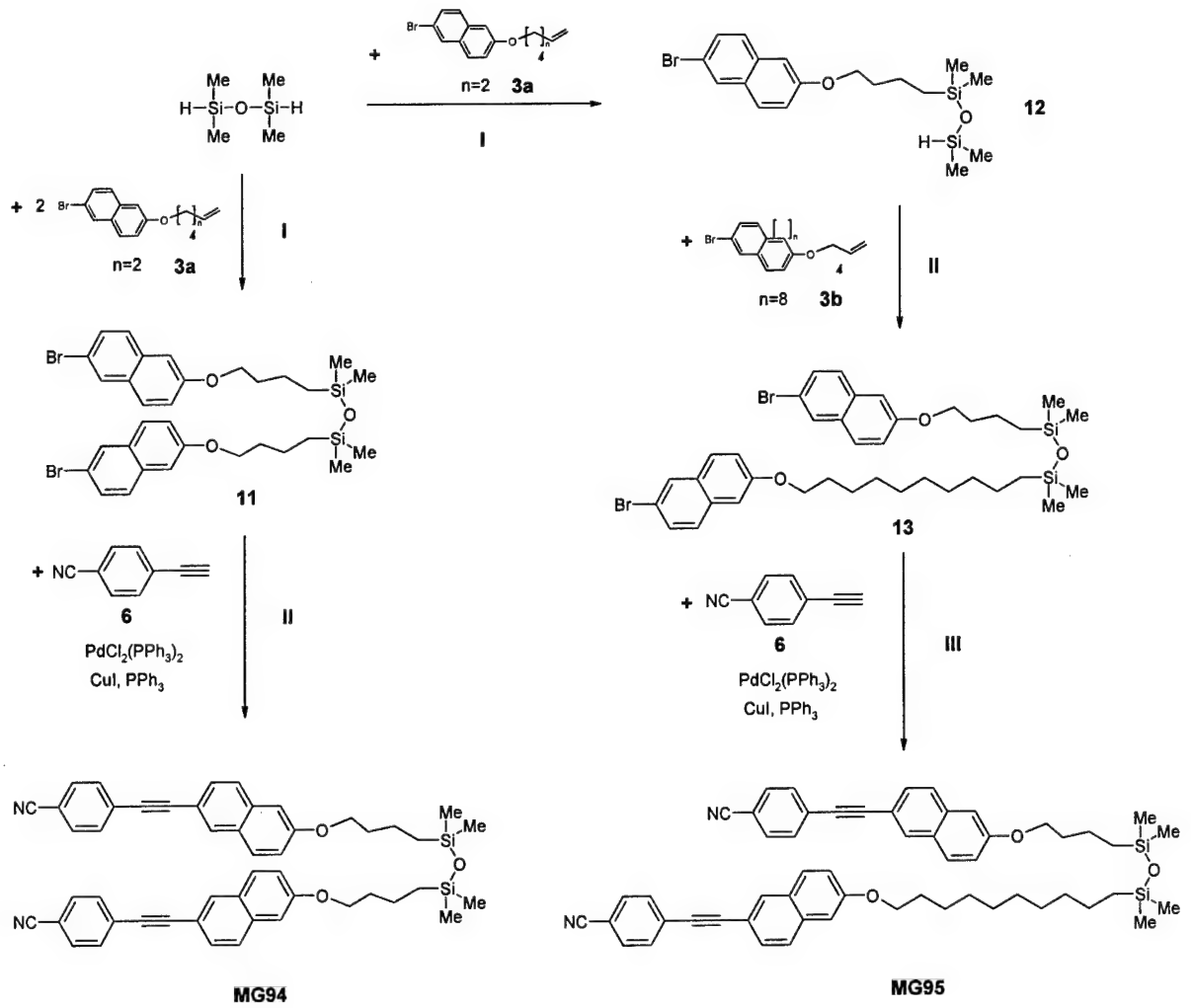

Scheme A1-3. *Synthetic pathway to bimesogenic siloxane-functional napthylene cyanotolanes.*

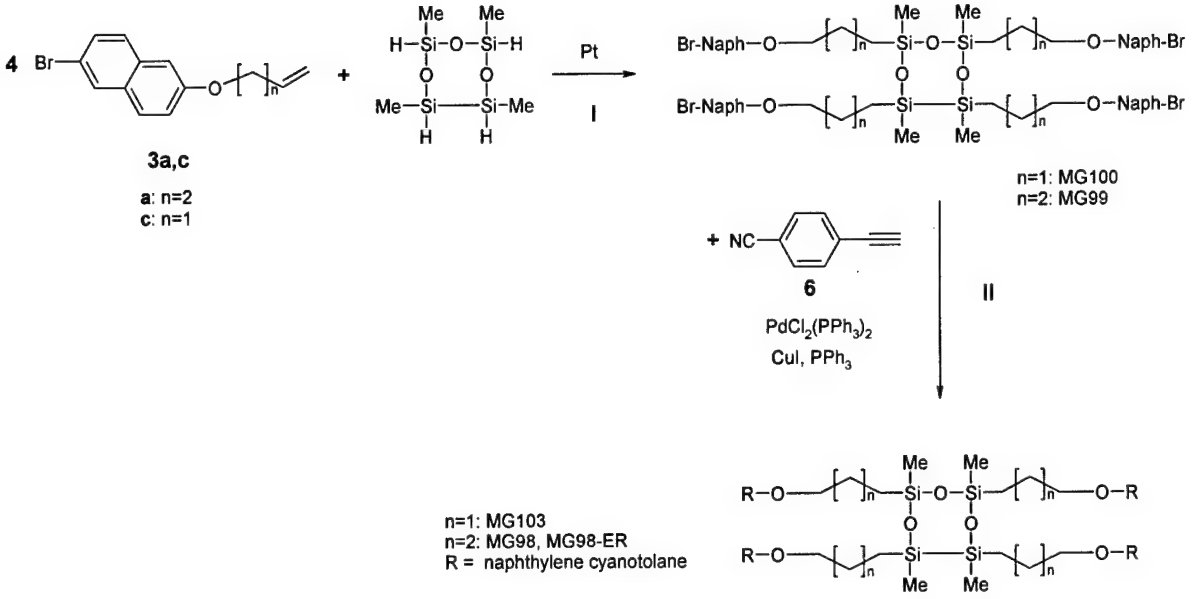

Scheme A1-4. *Synthetic pathway to cyclosiloxane napthylene cyanotolanes.*

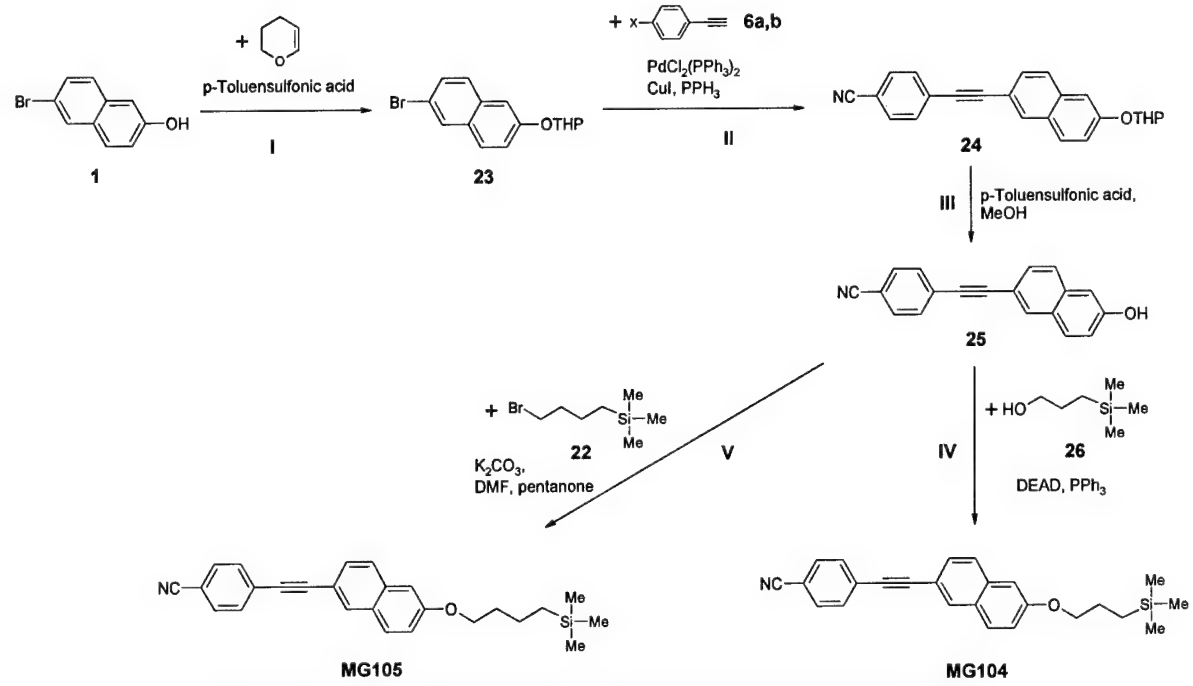

Scheme A1-5. *Synthetic pathway to silane-functional napthylene cyanotolanes.*

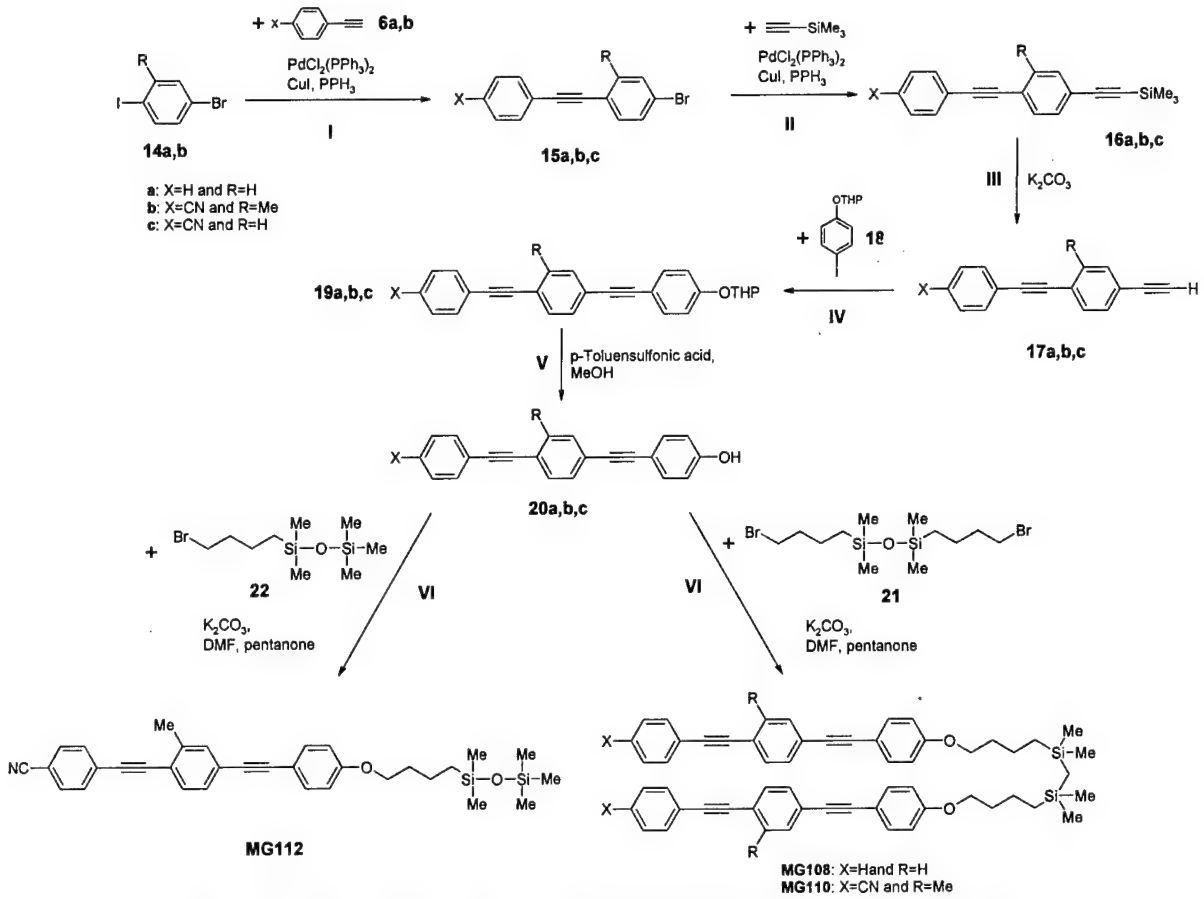

Scheme A1-6. *Synthetic pathway to bimesogenic siloxane-functional polytolanes.*

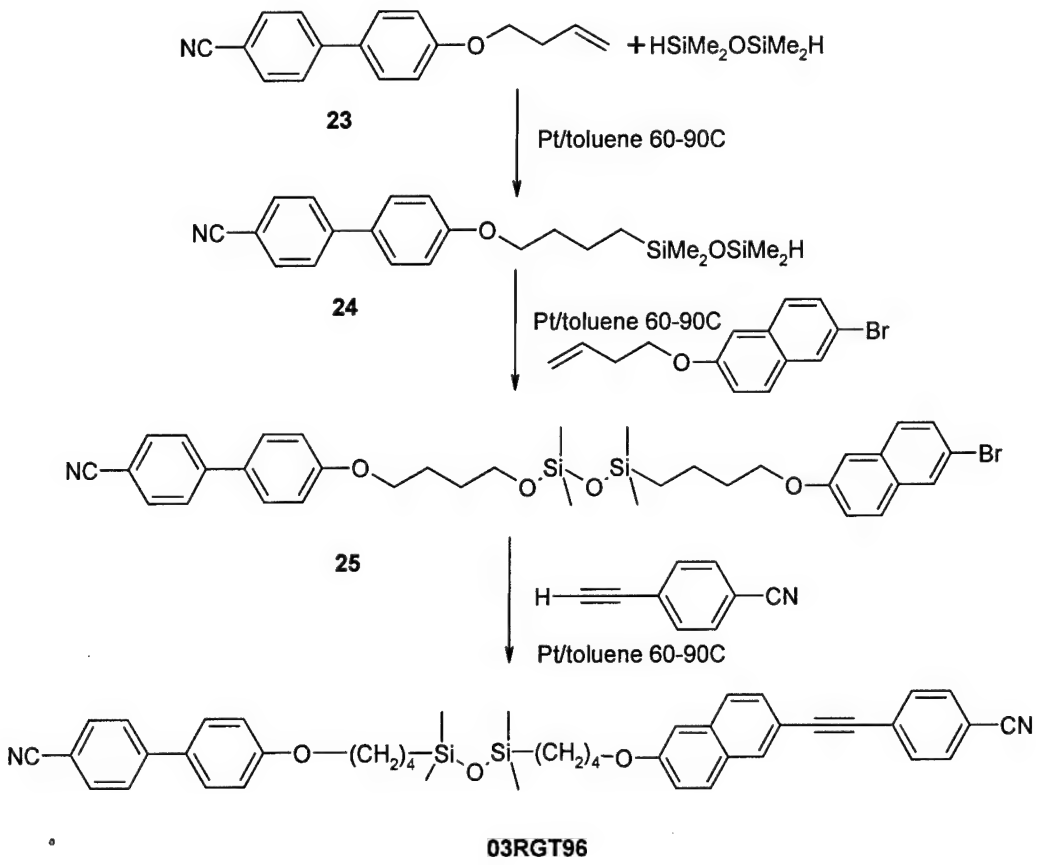

Scheme A1-7. *Synthesis of cyanobiphenyl/naphthylene cyanotolane ABC adduct - Product 03RGT96*

Appendix 2 – Phase Transition data for HCSFMs Exhibiting Liquid Crystal Phases

Naphthylene Cyanotolanes

Sample	Alkyl spacer	Si Moiety	Cycle	Phase Behaviour
MG92 FW 325	butenyl	NA	Heat Cool	Cr →102.6C (28.3) → N →164.3C (0.5) → I I → 163.5C (0.5)→ N → 48.2C (19.9)→ Cr
MG93 FW 409	decenyl	NA	Heat Cool	Cr1→66.5C (5.2) → Cr2 →71.2C (22.6) → N → 136.3(0.7)→I I → 135.4C(1.1)→ N → 34.3C (24.9)→ Cr
MG97-C FW 327	butyl	NA	Heat Cool	Cr1→ 105.9C (29.5) → Cr2 →111.5C (2.6) → N →185.1C(0.7)→ I I → 184.2C (0.8) →N → 83.8C (27.6) → Cr1
MG87-F3 FW 473	butyl	PMDS	Heat Cool	Cr →86.4C (30.1) → I I → 84.9C (2.9)→ Sa → 34.2C (20.6)→ Cr
MG88-F2 FW 547	butyl	HMTS (L)	Heat Cool	Cr→54.9C (18.3) → Sa → 66.5C(2.4) → I I → 65.1C(2.4)→ Sa → 23.7C (16.5)→ Cr
MG86-F3 FW 547	butyl	HMTS (P)	Heat Cool	Cr→113.6C (42.9) → I I → 55.4C(2.0)→ Sa → 22.8C (17.9)→ Cr
MG91-F2 FW 557	decyl	PMDS	Heat Cool	Cr1→ 33.3C(11.3) → Cr2 →57.0C (24.0) → Sa →118.4C(5.0)→I I → 117.3C(5.1)→ Sa → 33.0C (18.3)→ Cr1 → 16.2C (8.6)Cr2
MG90-F2 FW 631	decyl	HMTS (L)	Heat Cool	Cr→38.1C (14.7) → Sa → 106.3C(3.8) → I I → 105.4C(3.7)→ Sa → 26.9C (14.8)→ Cr
MG89 FW 631	decyl	HMTS (P)	Heat Cool	Cr→58.8C (33.9) → Sa → 103.7C(3.6) → I I → 102.6C(3.6)→ Sa → 27.2C (13.9)→ Cr
MG94 FW 784	butyl, butyl	TMDS	Heat Cool	Cr1 →75.6C (8.5) → Cr2 → 87.4 C (1.2) → Sa →123.7C(3.8)→I I → 123.5C (4.1)→ Sa → *→ Cr (* = slow cystallisation at room temperature in LC cell)
MG95 FW 868	butyl,decyl	TMDS	Heat Cool	Glass →35.6C (9.3) → Cr→56.0C (10.7) → Sa → 146.4C(5.0) → I I → 143.0C(4.9)→ Sa → -12C → glass
03RGT96 FW680	Butyl, butyl(CB)	TMDS	Heat Cool	Glass → -12.7C →Sa → 96.3C (0.4) → N → 105.4C (0.8) → I I → 104.7C (1.6) → N → 95.0C (1.0) → Sa → -15.4C → glass
MG98ER FW 1521*	butyl	D_{4H}	Heat Cool	glass → -2.6C → X → 70.3C & 78.3C (21.0) →N → 89.8C-127.1C→I I → 106.8C (0.3) → N → 52.7C (14.8) →X → 2.9C → glass
MG103 FW 1465*	propyl	D_{4H}	Heat Cool	glass → 84.8C → N → 106C (2.8) → I I → 110.9C (4.8)N →59.0C → glass
MG104 FW 385	propyl	Me3Si	Heat Cool	Cr → 139.9C (34.1) → I I → 103.4C (0.4) → N → 91.6 (28.7)→Cr
MG105 FW 399	butyl	Me3Si	Heat Cool	Cr → 94 - 100C (23.4) → I I → 89.4 (0.05) → N → 68.6 (2.2)→Sa → 54.7C (21.3)→ Cr

Table A2-1. *Liquid Crystal phase behaviour of siloxane- naphthylene cyanotolanes adducts. Enthalpy changes in kJ/mol.*

Note: PMDS = Pentamethyldisiloxane
HMTS = Heptamethyltrisiloxane; (L) = linear adduct, (P) = pendant adduct.
TMDS = Tetramethyldisiloxane
D4H = tetramethylcyclosiloxane
Butyl(CB) = 4-butytloxy-4'-cyanobiphenyl
***FW calculated using % of bromo-naphthylene and naphthylene cyanotolanes sites, based upon 1H NMR analysis**
****Cr1 and Cr2 phase assignments based on DSC data, no clear textural transitions observed by TOA.**

Polytolanes

Sample	Si Moiety	Cycle	Phase Behaviour
MG108 FW= 830	TMDS	Heat Cool	Cr → 154.9C (41.9) → I I → 150.0C (42.0) → Cr
MG110 FW = 908	TMDS	Heat Cool	Cr → 64C (13.6) and 70C (11.3) → N →204C (2.2) → I I → 197C (1.0) → N → 28.1C (11.7) and 23C (3.0) → Cr
MG112 FW = 520	PMDS	Heat Cool	Cr → 79.0C (18.0) → Sa → 132.8C (2.4) → I I → 128.0C (1.8) → Sa → 31.6C (14.8) → Cr

Table A2-2. *Liquid Crystal phase behaviour of siloxane-polytolane adducts. Enthalpy changes in kJ/mol.*

Appendix 3 – Experimental Techniques used to Determine Birefingence

A3-1. Sample Alignment

Siloxane samples responded poorly to the polyimide alignment coating within our commercial cells, which provided planar alignment, but with no preferred long range director orientation. Alignment was much improved with the use of a PTFE layer applied by rubbing a PTFE rod across glass slides at an elevated temperature of 300°C. A typical texture is shown in Figure A3-1. The defects are most likely due to limitations of the deposition process. Further research to produce defect free PTFE films for aligning siloxane containing liquid crystals is recommended.

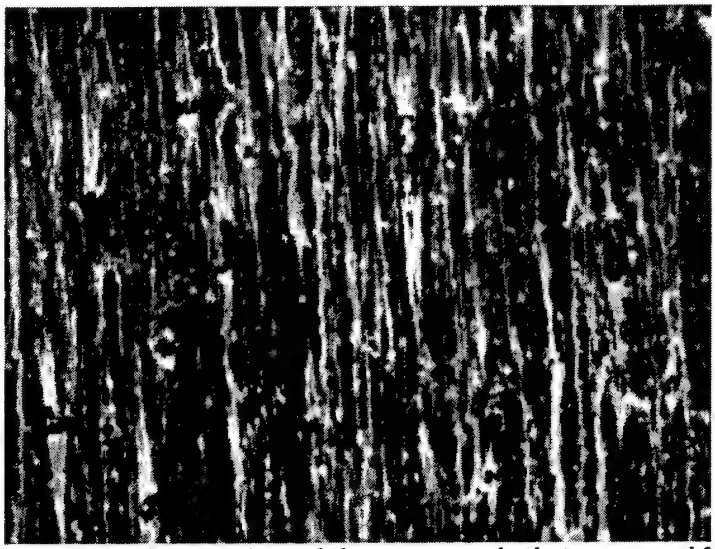

FigureA3-1. *Organosiloxane (MG88-F2) sample between crossed polarizers, rotated for minimum light transmission. The sample was contained in a cell of 10μm in thickness and with anti-parallel rubbed PTFE alignment.*

With the samples rotated for maximum transmission between crossed polarizers the alignment appears very uniform.

A3-2. Advanced techniques
A3-2a. The Hollow Prism Method

We begin this section by presenting a very simple and direct measurement technique of the refractive index. The method relies upon a comparison between the refracting angle of a prism filled with air, to a prism filled with liquid crystal. The alignment must be planar and of reasonably good quality, since any light scattering domains will introduce uncertainty into the measurement of the angles, by scattering the probing laser beam.

Figure A3-2 is a diagram of a hollow prism, filled with liquid crystal. We may construct such a prism by fabricating a wedge shaped cell, with the cell walls angled at typically 1 or 2 degrees. In our experiments we use a 10mW He-Ne laser, passing circularly polarised, 632.8nm light through the cell,

where the position of the laser beam is measure along a plane perpendicular to the path of the laser beam, by a photodiode attached to a travelling micrometer stage. In this way the relative positions of the beams deflected by the hollow prism may be measured to 0.001cm. Measurements are made with reference to the position, on our scale, of laser beam unhindered by the cell.

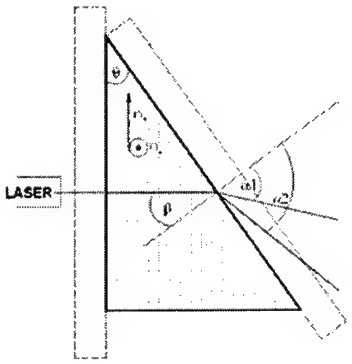

Figure A3-2. *Cross section through a hollow prism, in the form of a wedge shaped liquid crystal cell. Wedge angles of 1 or 2 degrees are typical.*

Making the assumption that $n_{air} \approx n_{vacuum} \approx 1$ Snell's law may be rearranged to give:

$$n_{e,o} = \frac{\sin \alpha_1, \alpha_2}{\sin \theta_{\{=\sin \beta\}}} \qquad \text{(A3-1)}$$

With the cell unfilled there will be two laser spots visible in front of the cell, one due to the direct beam and the other due to the beam reflected first from the front, angled surface and then reflected a second time from the back surface. The angle between them is equal to twice the wedge angle. The cell is filled in the isotropic phase and the direct beam is shifted. This new angle leads us to the refractive index of the isotropic phase from Equation A3-1. In an aligned birefringent mesophase the beam splits into two beams of orthogonal polarisation. The beam refracted at the greatest angle is the extraordinary ray and measurement of it leads to the extraordinary refractive index via Equation A3-1. In the same way measurement of the ordinary ray angle leads to the ordinary refractive index. Measurement of the actual angles requires measurement of the distances between the cell and the photodiode and taking the tangent of these, with associated inaccuracies in this process. This step may be avoided by simply using the measurement of the distance traveled by the photodiode (between the direct beam position and the new laser spot) in place of the actual angles, since transforming this distance into the actual angle is the same process for each angle and may therefore be mathematically eliminated.

A3-2b. Interference Method

We may use a polarizing microscope[5] in conjunction with a spectrometer[6] to measure the refractive indices of a liquid crystal by comparing the wavelength of interference of light in empty and filled cells respectively. The second polarizer (analyser) must be removed.

[5] Olympus BH-2 polarizing microscope, with Linkam Ltd. hot stage mounted on rotatable plate.

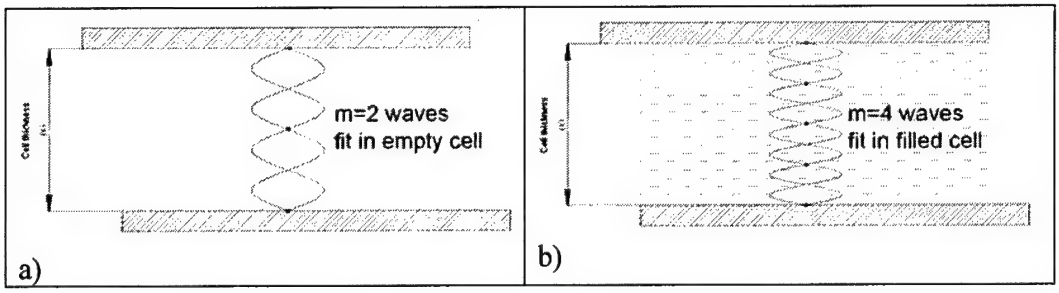

Figure A3-3. *a) Empty cell acting as a Fabri-Perot etalon. b) Filled cell, with interference wavelength now reduced from a).*

Light incident upon an empty cell will interferer with itself at some wavelength, and this may easily be observed if the cell is fairly flat and not too thick (≤25μm). The condition for interference is given by the usual Fabry-Perot etalon equation:

$$m\lambda = 2x\cos\theta\,, \qquad \text{(A3-2)}$$

where m is the integer number of wavelengths that fit inside the cell, λ is the wavelength of interference and x is the cell thickness. We make our measurements at normal incidence and therefore may set $cos\theta$ equal to 1.

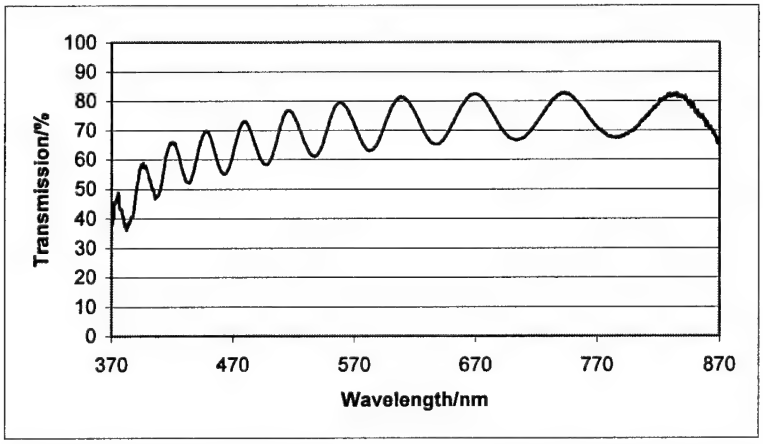

Figure A3-4. *Interference spectrum of white light transmitted through a liquid crystal cell.*

A typical spectrum is shown in Figure A3-4. We note the (full width at half maximum) wavelength at which a maximum is observed and plot these with the number of wavelengths that fit inside the cell (m), as in Figure A3-5.

[6] Ocean Optics USB2000, miniature fibre optic spectrometer.

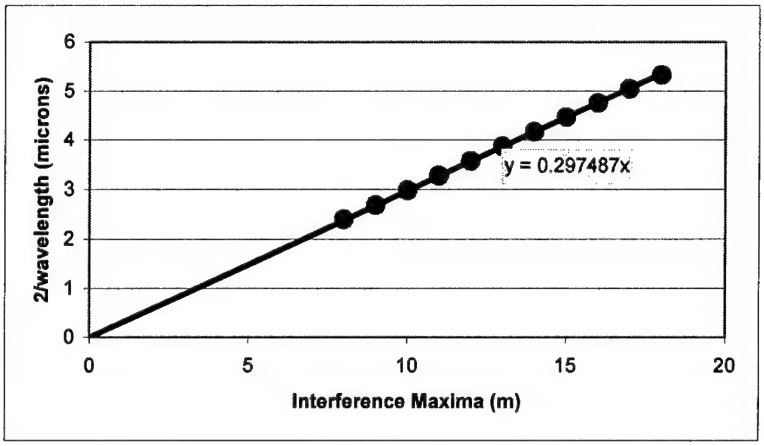

Figure A3-5. *Data derived from figure 5. The gradient of the graph is equal to the inverse of the cell thickness. The x-axis of the graph shown has been shifted following measurement of the cell thickness, to give the correct values (see text).*

Whilst we are initially ignorant as to the value of m, we may number the maxima with any consecutive values, without changing the gradient of Figure A3-5, which is equal in value to the inverse of the cell thickness, since a rearrangement of Equation A3-4 gives us a $y = mx + c$ type equation:

$$m\frac{1}{x} = \frac{2}{\lambda} \qquad \text{(A3-3)}$$

We may insert the cell thickness back into Equation A3-4 to obtain the proper value for the interference maxima. If we now fill the cell with liquid crystal we may observe a spectrum similar to Figure A3-4 if the electric field vector of the incident light is parallel or perpendicular to the optic axis of the liquid crystal. If this is not the case then the spectrum will be some superposition of these two *different* spectra, i.e. for light polarised parallel and perpendicular to the optic axis. If we were to plot Equation A3-5 for the two new spectra then we would be presented with a curve, rather than a straight line and this is due to the frequency dispersion of the liquid crystal. This complication translates into our being unable to determine m using the previous approach. If we were able to tabulate the m-λ relation, we may observe the change in interference wavelength between the case of the empty cell, the case of light with electric field vector experiencing ordinary refractive index and the case of extraordinary refractive index respectively, for a given m. Expressing this by using Equation A3-2 we have for the refractive index n:

$$n = \frac{\lambda_{empty}}{\lambda_{e,o}} \qquad \text{(A3-4)}$$

In order to find m (from Equation A3-2) in the case of the full cell (and therefore find $\lambda_{e,o}$) we must make a second measurement, e.g. using the hollow prism method. We find that reducing the cell thickness increases the spacing between possible values of m and thus we may be very confident of making accurate measurement with particularly thin cells (<~3μm), once we have obtained an approximate value by another method.

This method suffers from, in addition to the need for prior knowledge of approximate refractive index, somewhat time consuming data analysis and one is limited to measuring the refractive index at the interference wavelength and there will be few of these in thinner cells. It may therefore be necessary to make an accurate measurement of some wavelength using a thin cell and then measure the dispersion and temperature dependence, for example, using a thicker cell.

The major advantage of this method is that measurement under microscope allows us choice over the area of the sample to measure, which is useful if the sample quality varies across the cell. In addition any unexpected phase changes, or changes in texture induced by other means, may be readily observed.

Rotating Analyser

If a birefringent sample is placed between crossed polarisers and the analyser is rotated then the modulation in light intensity, detected after the analyser, will be a function of the birefringence and given by,

$$I = \frac{I_0}{2}\left[1 + \sin\left(\frac{2\pi}{\lambda}\Delta n \cdot x\right)\sin(\omega t + \alpha)\right], \qquad \text{(A2-5)}$$

where I_0 is the initial light intensity, the argument of the first sine term is the retardance (Equation A3-6), and gives an amplitude term, and the second sine term is the frequency term. The polarizer causes modulation at twice the rotation frequency and ω is therefore twice the rotation angular frequency, t is the time and α is a phase factor.

The input light source is a tunable Helium-Neon laser[7] (A) that allows selection of wavelengths at 632.8nm (red), 612nm (orange), 604nm (orange-yellow), 594nm (yellow) and 543nm (green). Light from the laser is directed through a piece of rotatable Polaroid (B), to allow control over the initial intensity, a Glan-Taylor polarizer[8] (C), to precisely define the laser polarisation, two irises (D) are used in conjunction with a 5cm focal length lens (E), to narrow the beam, a Fresnel Rhomb (F) is used to generate circular polarised light, and finally the light passes into the sample, which is held on a hot stage[9] (G). After the sample, light may either be directed into a spectrometer[10] (H), by a removable mirror, or pass through a piece of Polaroid mounted on a DC motor[11] (I) and detected by a battery powered photodiode (K), with interference filters mounted on a filter wheel in front of the diode (J).

---

[7] Research Electro-Optics Inc, LSTP-1010 – supplied by Laser 2000
[8] Optics supplied by Laser 2000
[9] Linkam Ltd.
[10] Ocean Optics USB2000, miniature fibre optic spectrometer.
[11] Mechanical Work Shop, Department of Physics and Astronomy, University of Southampton.

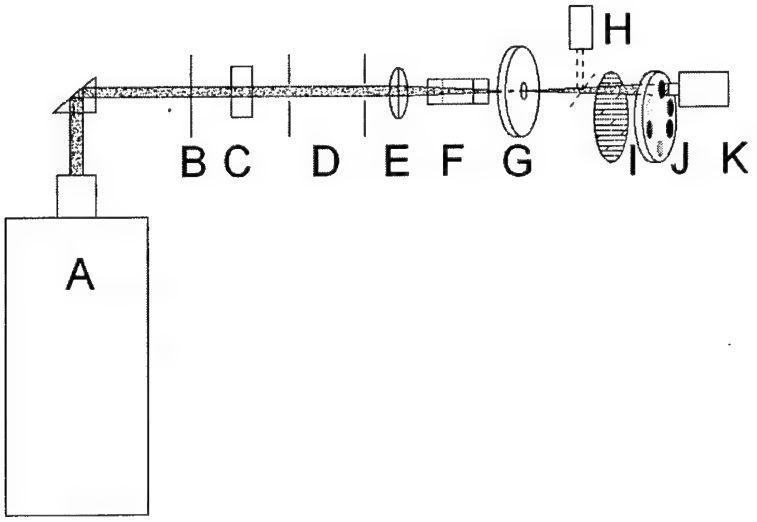

Figure A3-6. *Schematic of the rotating analyser experiment.*

The output signal from the photodiode is measured using an oscilloscope[12], connected to a PC via an RS232 cable, where the raw voltage levels are recorded. The oscilloscope is triggered by the signal from an LED and photodiode either side of the rotating analyser. The spectrometer is used to measure the cell thickness in exactly the same way as in the case of the interference method. It would be possible to use the interference method and the rotating analyser method on the same piece of equipment if the sample were mounted on a rotatable stage.

A C++ program was written to fit Equation A3-9 to the data from the oscilloscope, using the Levenberg-Marquardt method[13] for data fitting. Input into the program are the frequency of the rotating analyser, I_0 and the list of voltage levels; all of which are recorded automatically by the oscilloscope by means of a second program. The second program is written in Visual Basic and acts as a 'windows' style interface between user and C++ program. The value of sin δ is accurately fitted by the program (Figure A3-7), unfortunately the function sin δ is multi-valued and we once again require a method, such as the hollow prism, to gain an approximate value for the birefringence (from which we can obtain an approximate value for δ from Equation A3-6). The rotating analyser therefore presents us with δ_0 from Equation A3-6, rather than the true retardance i.e.

$$\sin^{-1}(\sin\delta) = \delta_0 \pm m\pi \qquad \text{(A3-6)}$$

Once again we may assist arriving at the correct value of the birefringence by using a thin cell, since the spacing of these possible values increases with decreasing cell thickness and increasing wavelength, however, we are not presented by any disadvantages of using thin cells in this case. It should be noted that the error of the measurement increases where sin δ has its maximum and minimum values. These should be between 1 and -1, however the actual value reached is usually

[12] Agilent 52624A
[13] Press W.H. *Numerical Recipes in C, second edition.* Cambridge University Press (January 1993).

somewhat less than this, with the resulting reduction in accuracy. It is our opinion that replacing the rotating piece of Polaroid, with a higher extinction ratio polarizer would alleviate this problem.

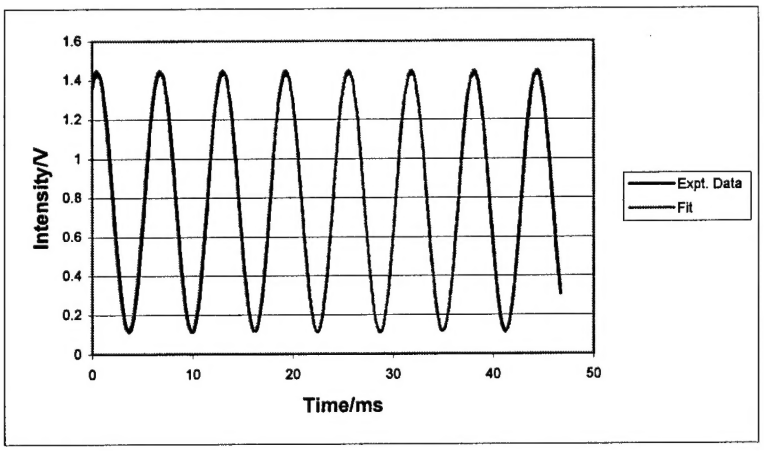

Figure A3-7. *Voltage data plotted with the fit generated by a computer program using the Levenberg-Marquardt method, for the rotating analyser experiment.*

The rotating analyser experiment has the advantage of providing δ_0 values very quickly (~5 seconds per data point and would be quicker with a GPIB interface between PC and oscilloscope, rather than the RS232 presently used); it is very sensitive to changes in birefringence, so we are therefore able to measure birefringence as a function of applied fields or as a function of changes in temperature; and the phase α is related to the angle of the optic axis.

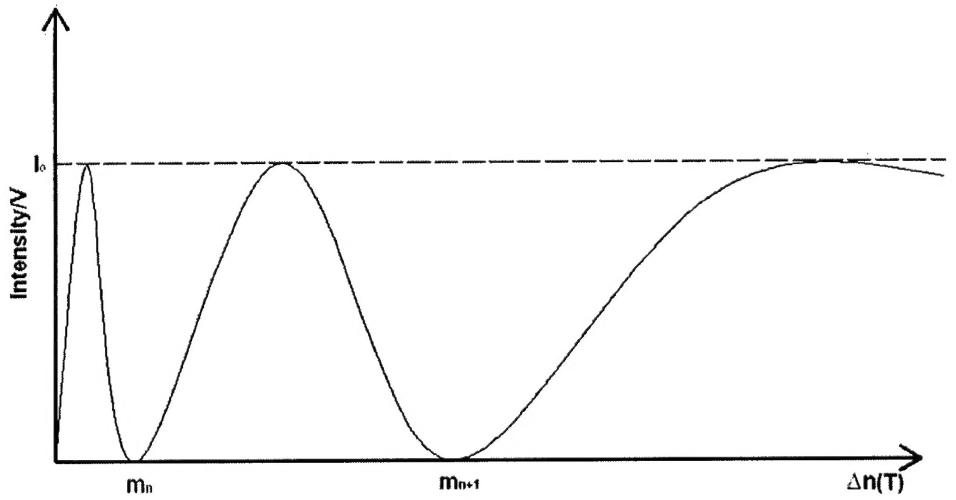

Figure A3-8. *Variation of signal amplitude, at the photodiode, with temperature. The m_n correspond to the m values in equation 6.*

Since we are able to measure the angle of the optic axis we may investigate in-plane switching phenomenon such as ferroelectric and flexoelectric tilt angles. The switching angle may be measured

by taking the phase change (ΔT) upon switching and the period (T) of the trace, from the oscilloscope and using the relation:

$$\phi = \frac{\Delta T}{T} \cdot 90, \qquad \text{(A3-7)}$$

The amplitude of the signal at the photodiode (Figure A3-7) will periodically change with birefringence and therefore also with a change in temperature. This is represented in Figure A3-8. Unfortunately we may not take advantage of this for measuring the absolute retardance, i.e. by counting the number of minima from the isotropic phase which has zero birefringence. This is because of the discontinuous (first order) phase transition, between the isotropic phase and the mesophase, in which the birefringence jumps discontinuously and we can not know how many minima have been "missed" during the phase transition. If we were to use a more advanced sample holder and temperature controller, so that very slow (~0.05°/min) cooling rates were obtainable, then there is evidence that, in spite of the transition being first order, we would be able to track a continuous optical transition from the isotropic phase and thus be able to measure m by counting the peaks directly.

Appendix 4- Analysis of the Electro-Optical Effect

The relative contributions of birefringence (refractive index change) and thickness change toward the change in refractive power of the lens material can be determined from changes $\Delta(nh)$ in the optical path length nh – sometimes called optical constant. $\Delta(nh)$ consists of two parts, $\Delta n/n$ and $\Delta h/h$, which separately describe the contributions from refractive index and thickness changes.

The treatment of thickness change $\Delta h/h$ has been previously discussed in Section 2.B. Substituting values $\varepsilon_r = 2.5$, $E_Y = 3$ kPa, and at $E = 2.3$ V/μm (3500 V across 1.5 mm) in Equations (6) and (7), the theoretical thickness change $\Delta h/h$ is expected to be –0.021 or compression by 2%. Taking into account that a portion of liquid crystal added to the formulation is ineffective and that the usable refractive index difference $\Delta n_{LC} = 1.594 - 1.532 = 0.062$ for K15, and the expected refractive index change in a PDLC material in which all droplets are oriented parallel to a sufficiently high electric field is

$$\Delta n^{\text{eff}} = -\Delta n_{LC} \cdot c^*_{LC} = -0.062 \times 0.07 = -0.004. \qquad (1)$$

Hence, the total effect on the optical path length, $\Delta(nh)/nh$, can be estimated as

$$\Delta(nh)/nh = \Delta n/n + \Delta h/h = (-0.004)/1.594 + (-0.021) = -0.003 - 0.021 = -0.024 \qquad (2)$$

which shows that under the given conditions of K15:MP1200 PDLC lens demonstration, the effect from the orientation of the LC droplets in the applied electric field is negligible and the refractive power change of the lens is predominantly due to the lens deformation. Considering that the tension of 3500 V applied across a distance of 1.5 mm results in an electric field of E = 23 kV/cm which is already above the dielectric strength of dry air, the value predicted by Equation (2) must be taken as an upper limit.

Using the values obtained for Δn and Δh, one can deduce the change in focal length of this PDLC lens. The initial focal length is calculated to be 18.8 mm while at 3500 V, it is expected to be 19.5 mm resulting in approximately 4% change.

The refractive index of the PDLC material can also be measured experimentally. The refractive index of K15:MP1200 PDLC at various mesogen loadings was measured using the prism-coupling technique. At 35% K15 loading of the PDLC formulation, the refractive index change from the unbiased state to a field strength of 2.3 V/μm applied on the PDLC lens is expected to be approximately 5×10^{-4}. Due to the geometry of the measurement, the index change measured was along the longitudinal axis of the mesogen (i.e., parallel to the electric field direction) and is normal to the direction at which PDLC lens would be used. Nevertheless, one can extract the index change expected in the transverse direction by normalizing with the ratio of Δn expected in the longitudinal and transverse directions

$$\Delta n_{sh}/\Delta n_{lg} = (n_{sh} - n_{avg})/(n_{lg} - n_{avg}) = -0.062/0.124 = 0.5. \qquad (3)$$

Hence, Δn in the direction normal to the applied electric field would be approximately 2.5×10^{-4} which is significantly smaller than the theoretically determined value of 4×10^{-3}. Although the actual thickness change is unknown, its contribution is believed to be greater than that from the refractive index change judging from the observed distortion and the index change value.